HEAT TRANSFER PREDICTION IN A SHALLOW CAVITY EFFECT OF INCOMING FLOW CHARACTERISTICS

by

Fatima MADI AROUS

LMFTA, Faculty of Physics, University of Sciences and Technology
Houari Boumediene, Algiers, Algeria

Original scientific paper
DOI:10.2298/TSCI140119093M

This study deals numerically with a heat transfer in a turbulent flow over a shallow cavity. Two different configurations of the incoming flow are considered: a boundary layer flow and a plane wall jet flow, in order to examine the wall jet outer layer effect on the heat transfer. This layer is an important additional turbulence source in the wall jet flow. Reynolds number and turbulence intensity effects were investigated in the boundary layer incoming flow case. The cavity depth to nozzle height ratio effect was examined in the wall jet incoming flow case. The numerical approach is based on k-ω standard turbulence model. This study reveals that the heat transfer is very sensitive to the incoming flow characteristics. The turbulence intensity increase accelerates the reattachment of the shear layer at the cavity floor and enhances the heat transfer. The reattachment phenomenon seems to be less affected by the Reynolds number. However, an increase in this parameter ameliorates the heat transfer. It was also observed a heat transfer enhancement in the wall jet incoming flow case as compared to that of a boundary layer. Likewise, it was found that the augmentation of the cavity depth to the jet nozzle height ratio improves even more the heat transfer. The maximum heat transfer occurs upstream of the reattachment.

Key words: *cavity flow, boundary layer, wall jet, heat transfer, recirculation, reattachment*

Introduction

Flows characterized by the separation and recirculation phenomena, as flow over cavities and steps or around obstacles, promote mixing fluid and can play an important role in heat transfer. This kind of flows is of a great interest as it is related to various engineering applications such as cooling systems for electronic components, combustion chambers, heat exchangers and solar energy collectors. Mehrez *et al.* [1] have examined flow control and mass transfer in separated and reattached flow over a backward facing step. The flow control is realized by the introduction of a periodic local perturbation at the step edge. Results show important changes in flow characteristics and an enhancement in heat transfer due to the applied perturbation. Lancial *et al.* [2] have investigated experimentally and numerically the effect of a turbulent wall jet on heat transfer over a non-confined backward facing step. It was found that the reattachment length is between 4.2H and 4.33H which is shorter than that of a confined backward facing step. The Nusselt number, low in the recirculation region, increase to a maximum value in the reattachment

* Author's e-mail: madi.fatima@yahoo.fr; f.madi@usthb.dz

zone and decrease within the recovery region. Mushatet [3] has considered a turbulent flow over a backward facing step with turbulators ribs. This purpose was to investigate the ribs effect on flow characteristics, principally on the recirculation zones size and on the heat transfer. It was found that the turbulators ribs enhance significantly the heat transfer. The size of the recirculation zones increases with the step height. The heat transfer enhances with the increase of the Reynolds number, the step height and the number of ribs. Turbulators ribs are widely used in several engineering applications such as serpentine cooling air and gas turbine. However, the flow field between two roughness elements is similar to a cavity flow, Oka [4]. Many studies were conducted to investigate the cavities effect on flow and heat transfer. Richards *et al.* [5] experiments show that the heat transfer is very sensitive to the cavity aspect ratio but is less affected by the inlet boundary layer thickness. The study of Aung [6], concerning a laminar forced convection in cavities with aspect ratios of 1 and 4, show that the temperature distribution outside the cavity is less affected by the flow inside the cavity. In the cases considered in this study (AR = 1, 4), the maximum heat transfer on the cavity floor is located between the midpoint of the cavity floor and the downstream wall. Everywhere on the cavity floor, the local heat transfer is substantially less than that of the upstream cavity region. Batthi and Aung [7] studied numerically, by finite difference analysis, the laminar flow over rectangular cavities. The results indicate that while the average Nusselt number in the cavity is related to the Reynolds number raised to a power law, the latter depends on the aspect ratio and varies between the cavity floor and the side walls.

The study of Aghajani Delavar *et al.* [8] deals with the effect of the heater location on flow field, heat transfer and entropy generation in a cavity. The results show that the heater location has a main effect on the flow pattern and on temperature distribution in the cavity. Higher heat transfer was observed from the cold walls when the heater was located on the vertical wall. The heat transfer increases from the heater surface when it is located on the horizontal wall. Stalio *et al.* [9] have studied numerically a forced convection on a channel with a periodic series of shallow cavities at low Prandtl number. It was observed that, in laminar flow conditions and for isothermal walls, the presence of the cavity has a negative effect on heat transfer due to the presence of a stable vortex downstream the backward step. The insulating effect of the vortex increases with the Reynolds number. The only case where the global Nusselt number increases with the Reynolds number is due to a heat transfer enhancement in the developing boundary layer region downstream the cavity with an aspect ratio of 10.

The present study focuses on the upstream flow characteristics effect on shallow cavity flow behavior and on heat transfer. The cavities aspect ratio is AR = 10. The cavities walls temperature was fixed at T_w = 320 K and that of the inlet flow at T_0 = 300 K. The case studied experimentally by Esteve *et al.* [10] and numerically by Madi Arous *et al.* [11] has been used for the turbulence model validation. We used, in this study, the same geometric parameters of the reference [11]; therefore, we adopted the same turbulence model and scheme discretizations.

Theoretical formulation

The fluid is incompressible and the flow is assumed two-dimensional and statistically steady.

Governing equations

The mathematical model consisted of the following steady Reynolds averaged equations in Cartesian tensor form:

– continuity equation

$$\frac{\partial U_j}{\partial x_j} = 0 \tag{1}$$

– momentum equation

$$U_j \frac{\partial U_j}{\partial x_j} = -\frac{1}{\rho}\frac{\partial P}{\partial x_i} + \frac{\partial}{\partial x_i}\left[\nu \frac{\partial U_i}{\partial x_i} - \overline{u_i u_j}\right] \tag{2}$$

– energy equation

$$U_j \frac{\partial T}{\partial x_j} = \frac{\partial}{\partial x_j}\left[\alpha \frac{\partial T}{\partial x_j} - \overline{u_j \theta}\right] \qquad \text{where} \qquad -\overline{\rho u_j \theta} = \alpha_t \frac{\partial T}{\partial x_j} \tag{3}$$

The turbulent Prandtl number for energy transport equation is given by:

$$\alpha_t = \frac{\nu_t}{\mathrm{P_{rt}}} \tag{4}$$

where U_i is the velocity vector component in i direction, and P – the pressure, and $\overline{u_i u_j}$ represents the stress tensor.

Turbulence modelling

A cavity flow as a backward facing step flow is characterized by the presence of a shear layer and separation/recirculation phenomena. In the present study, we have considered a wall jet flow over a rectangular cavity. So, previous studies have shown that the *k-ω* model predicts fairly well the free shear flows, the mixing layers, the jets, the wall-bounded flows and the separated flows; for example, it predicts the backstep reattachment length within 4% of the measured one [12].

The numerical approach is realized by the Wilcox (1998) [12] version of the standard *k-ω* model. In addition to the turbulent kinetic energy equation, this model uses the specific dissipation rate equation.

The turbulence kinetic energy and the specific dissipation rate are given by eqs. (5) and (6), respectively:

$$\frac{\partial k}{\partial t} + U_j \frac{\partial k}{\partial x_j} = G_k - \Upsilon_k + \frac{\partial}{\partial x_j}\left[\Gamma_k \frac{\partial k}{\partial x_j}\right] \tag{5}$$

$$\frac{\partial \omega}{\partial t} + U_j \frac{\partial \omega}{\partial x_j} = G_\omega - \Upsilon_\omega + \frac{\partial}{\partial x_j}\left[\Gamma_\omega \frac{\partial \omega}{\partial x_j}\right] \tag{6}$$

where Γ_k and Γ_ω are the effective diffusivity of k and ω respectively; they are given by:

$$\Gamma_k = \nu + \frac{\nu_t}{\sigma_k}; \qquad \Gamma_\omega = \nu + \frac{\nu_t}{\sigma_\omega} \tag{7}$$

The G_k and G_ω characterize the turbulence kinetic energy and the specific dissipation rate generation, respectively, due to the mean velocity gradient (eq. 8).

$$G_k = \tau_{ij}\frac{\partial U_i}{\partial x_j}, \qquad G_\omega = \alpha\frac{\omega}{k}G_k \tag{8}$$

The Υ_k and Υ_ω represent the dissipation rate of k and ω, respectively. They are given by:

$$\Upsilon_k = \beta^* k\omega, \qquad \Upsilon_\omega = \beta_i f_\beta \omega^2 \tag{9}$$

where ν_t is the turbulent viscosity given by:

$$\nu_t = \alpha^*\frac{k}{\omega} \tag{10}$$

The σ_k and σ_ω are the turbulent Prandtl numbers for k and ω, respectively ($\sigma_k = \sigma_\omega = 2$).

The α, α^*, β, β^*, and β_i are closure coefficients. f_β is an auxiliary equation which include some corrections in the low-Reynolds number regions. These terms are detailed by [12].

Numerical procedure

Ansys 14.0 is used as a CFD solver. The discretization of the equations is based on the finite volume method with a co-located scheme. The PISO algorithm is used for the pressure-velocity coupling, the QUICK interpolation scheme is applied for the convection–diffusion interpolation term.

The near wall treatment is based on the enhanced wall functions by the application of a single law for the wall regions. This is achieved by the wall function proposed by Kader [13].

The calculation domains of the two configurations considered in this study are given in figs. 1(a) and 1(b).

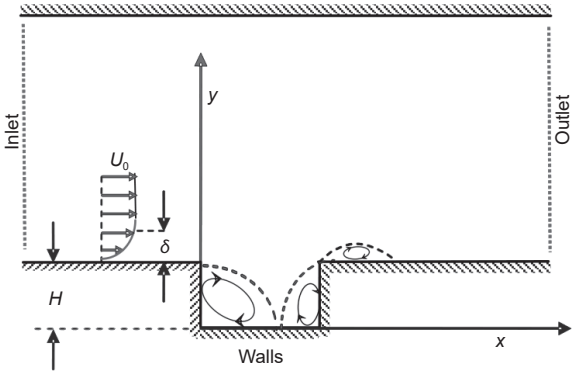

Figure 1(a). Schematic of calculation domain in the boundary layer incoming flow case

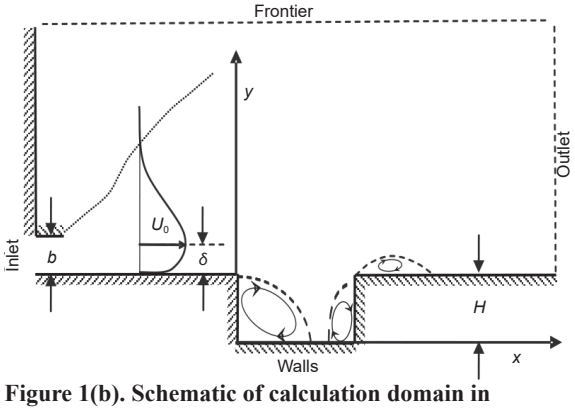

Figure 1(b). Schematic of calculation domain in the wall jet incoming flow case

Computational grids

The calculation domain is subdivided into two parts: the inner cavity region ($y/H < 1$) and the outer one ($y/H > 1$). The grids are Cartesian, non-uniform and sufficiently refined near the cavity walls where very high gradients prevail in the viscous sub-layer. The computational grid test is based on the boundary layer grid. Table 1 gives the nodes numbers of the grids test. The grid 2 gives a closest result to the experimental one and is used for the computation of the boundary layer case. The gridding of the wall jet cases is based on this grid by trying

to keep the same refinement near the walls, fig. 2. The near wall values of y^+ corresponds to $0.3 < y^+ < 13$ for all studied cases.

The *Nx* and *Ny* represent, respectively, the x-direction cell number and that of y-direction.

Table 1

Grid	Cavity ($y \le H$) (Ny) × (Nx)	Outer region (y > H) (Ny) × (Nx)
1	95 × 40	375 × 60
2	100 × 60	420 × 70
3	110 × 70	440 × 90

Solution convergence

The convergence of the numerical solution is based on scaled residuals; they are fixed at 10^{-6} for all governing equations. The solution is assumed to have converged when all these residuals are less than or equal to the prescribed value. Computations are carried out until the steady state is reached.

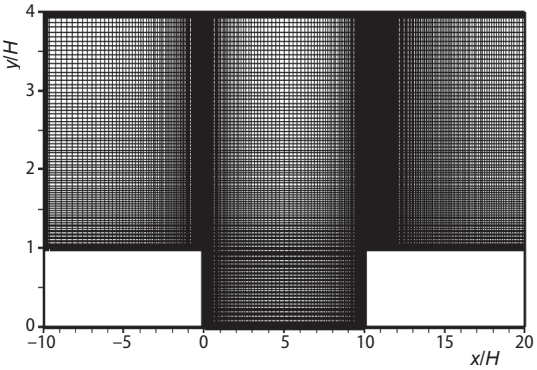

Figure 2. Computational grid

Boundary conditions

The boundary conditions imposed at the calculation domain frontiers are. At the inlet frontier and for each variable, uniform profiles are imposed:

$$U = U_{in}, \qquad V = 0, \qquad k_{in} = \frac{3}{2}(IU_{in})^2, \qquad \omega_{in} = \frac{\sqrt{k_{in}}}{\ell \sqrt[4]{C_\mu}} \qquad \text{and} \qquad T = 300 \text{ K}$$

where I is the turbulence intensity, ℓ a turbulence length scale, and C_μ a turbulence model empirical constant equal to 0.09.

At the outlet boundary and the upper frontier in the wall jet case, constant pressure is imposed.

At the wall boundaries, the no-slip condition is imposed, $U = V = 0$. The turbulent quantities correspond to the wall function approach. The cavity walls are maintained at a constant temperature $T = 320$ K and the other ones are adiabatic.

Results and discussions

Code validation

For the validation of numerical results we have considered the incoming flow conditions of Esteve *et al.* experiment [10]. The Reynolds number based on the cavity depth is 67000, the boundary layer thickness is about 20 mm and the turbulence intensity of the external flow is of 2%.

A preliminary comparative study of three turbulence models has been conducted: the standard *k-ω* model, the *k-ω* SST model and the low-Re stress-omega model. Figure 3 shows the mean flow structure inside the cavity predicted with the three models and the experimental one. The experiment shows the presence of an important recirculation bubble behind the upstream step and two others close to each corner. A small eddy is also observed on the downstream step. The length of the main recirculation zone is about 8.5*H*. The standard *k-ω* and the RSM

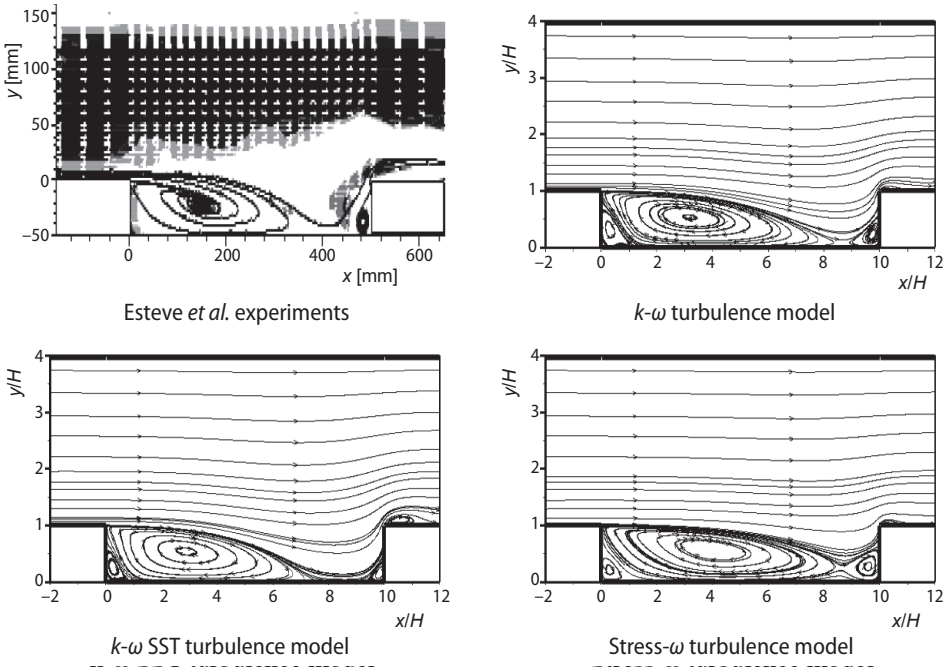

Figure 3. Comparison between the experimental cavity flow structure and the predicted ones

turbulence models allow finding the complex structure of the cavity flow with similar sizes of recirculation zones; they also predict a no-reattachment of the shear layer at the cavity floor as it was observed in the experiment. However, the *k-ω* SST predicts a shear layer reattachment and overestimates the size of the recirculation located above the downstream step.Therefore, we can conclude that the *k-ω* model gives satisfactory results in this flow type. Similar cavity flow structure has been evidenced by Avelar *et al.* experiments [14], by Zdanski *et al.* numerical results [15] and Madi Arous *et al.* numerical results [11] and [16]. The experiments of Oka [4] also show an analogous flow structure between two roughness separated by a distance of 9*H*.

The wall pressure coefficient is defined as:

$$C_p = 2\frac{P - P_{ref}}{\rho U_0^2}$$

where P_{ref} is the reference static pressure. P_{ref} is taken at the same position of the experiment.

Figure 4 compares computed and measured pressure coefficient at the cavity floor. This figure shows that the numerical results are in good agreement with the experimental ones. In this circumstance, the *k-ω* model gives the most satisfactory result.

Reynolds number and turbulent intensity effects

Reynolds number and turbulence intensity effect are examined in the boundary layer incoming flow case. Figure 5 represents the mean flow structure and the isotherms for different Reynolds number and turbulence intensity values. In all these cases, we note the presence of an important recirculation bubble just behind the upstream step and two vortices at the cavity corners in addition to a small vortex on the downstream step. This figure shows that the Reyn-

olds number variation does not affect much the flow structure while the turbulence intensity increase leads to a significant variation of the cavity flow behavior. Indeed, the turbulence intensity augmentation causes an important diminution of the principal recirculation bubble and accelerates the reattachment phenomenon. The same fact was observed by Zdanski *et al.* [15] in the case of a cavity with an aspect ratio of 8.

Figure 6 displays the skin friction coefficijent distribution at the cavity floor for different Reynolds number and turbulence intensity values. The many zero Cf points confirm the presence of several recirculation zones. We note that the turbulence intensity augmentation causes an important diminution of the principal recirculation bubble size. The size of this recirculation also drops when the Reynolds number increases; but this reduction is less significant than that causes by the turbulence intensity rise.

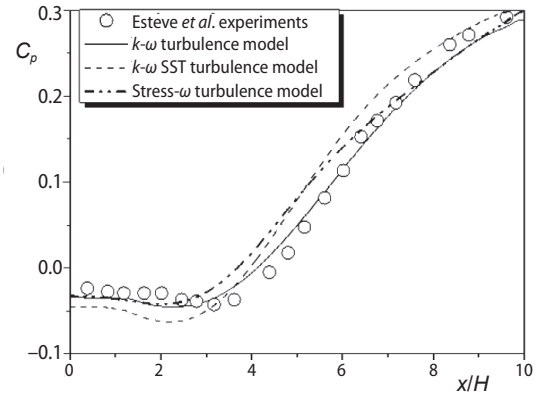

Figure 4. Pressure coefficient evolution at the cavity floor

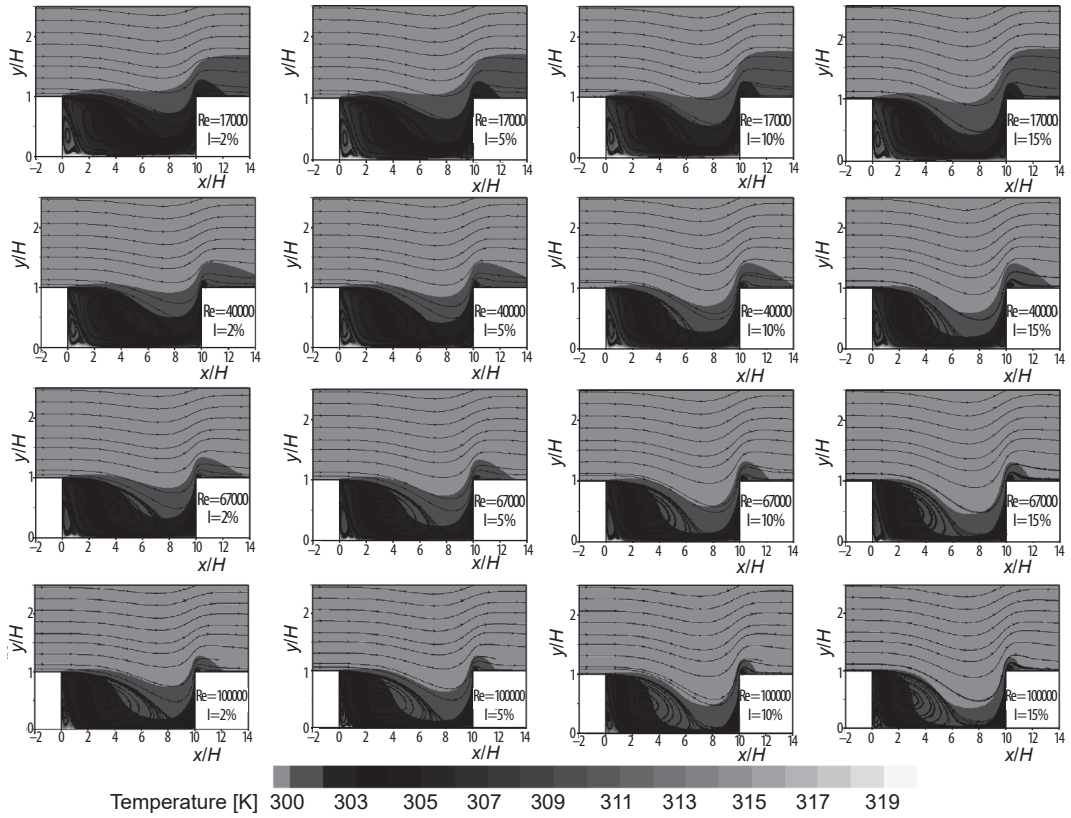

Figure 5. Cavity flow structure and isotherm for different values of Reynolds number and turbulence intensity

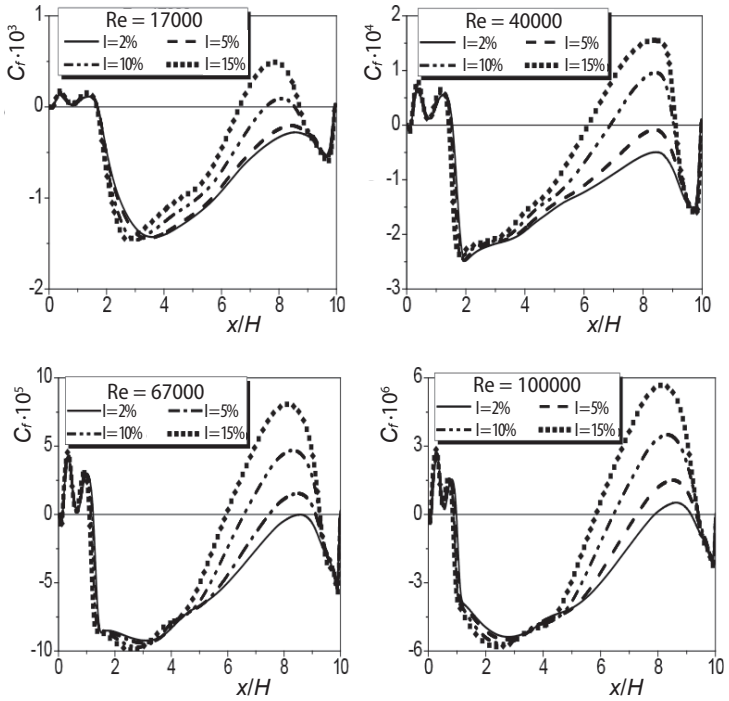

Figure 6. Skin friction coefficient profiles at the cavity floor for different values of Reynolds number and turbulence intensity

Figure 7 shows the evolution of the reattachment length at the cavity floor versus the turbulence intensity for four Reynolds number values. This figure depicts a reattachment length decrease with the turbulence intensity increase. However, the reattachment length variation is less important when the Reynolds number varies. The feeble influence of Reynolds number on a cavity flow with an aspect ratio of 12 was also evidenced by Zdanski *et al.* [15]. This study has shown that the Reynolds number effect is very important in laminar flow while it is much less in turbulent flow.

The heat transfer have been examined through the isotherms contours (fig. 5), the temperature profiles at several cavity sections (fig. 8), the evolution of the local Nusselt number at the cavity floor (fig. 9) and that of the maximum Nusselt number (fig. 10). Figure 5 shows that the isotherms follow the streamlines behavior. It displays the presence of a hot fluid layer within the cavity which extends up to above the downstream step. Increasing of Reynolds number and turbulence intensity causes a reduction in this hot fluid layer thickness. This reduction is more heightened by the turbulence intensity rise than by the Reynolds number increase, inside the cavity; however, the hot layer located above the downstream step is more sensitive to Reynolds number variation to that of turbulence intensity.

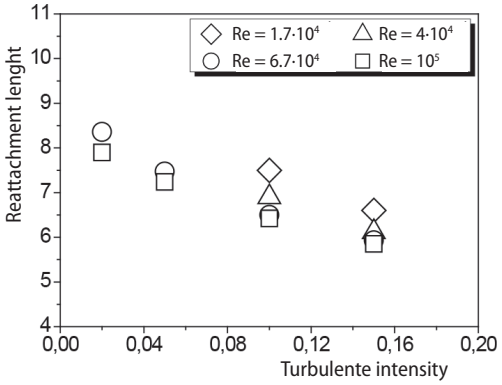

Figure 7. Evolution of the reattachment length with Reynolds number and turbulence intensity

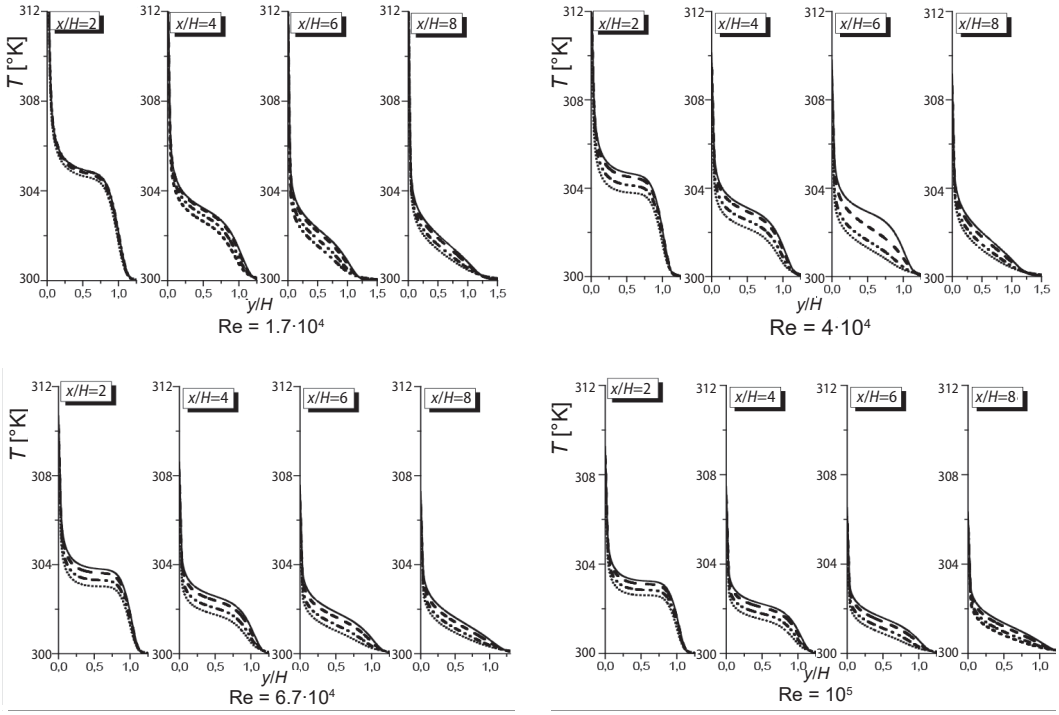

Figure 8. Temperature profiles at different cavity sections

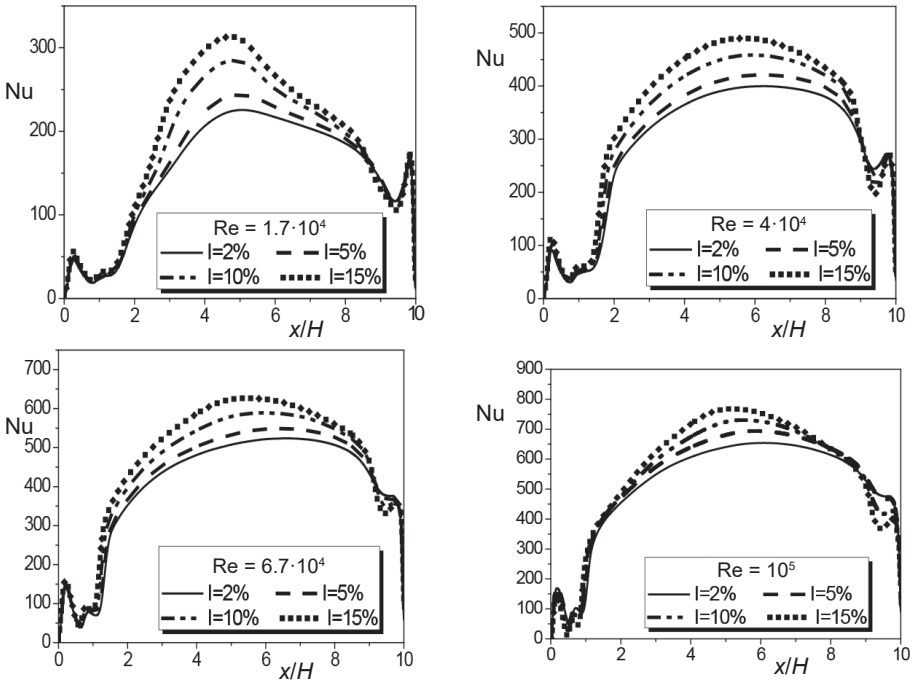

Figure 9. Nusselt number profiles at the cavity floor for different values of Reynolds number and turbulence intensity

Figure 8 shows that the highest temperatures are located at the vicinity of the upstream cavity corner where the fluid remains encapsulated in the recirculation bubble. This bubble constitutes a kind of thermal insulation. This same phenomenon was observed by Zdanski *et al.* [15]. The Reynolds number increase accelerates a temperature decrease inside the cavity. Particularly, in the vicinity of the cavity floor, where a net temperature drops is noted. Indeed, in the $x/H = 8$ section, we note a temperature decrease of 7 K when the Reynolds number value goes from $\mathrm{Re} = 1.7 \cdot 10^4$ to $\mathrm{Re} = 10^5$. The turbulence intensity increase also leads to a temperature drop, but with a lesser intensity than that caused by the Reynolds number augmentation.

The Nusselt number is defined as:

$$\mathrm{Nu} = -\frac{L}{T_w - T_0}\frac{\partial T}{\partial y}$$

where L is the cavity length. Figure 9 shows the distribution of local Nusselt number along the cavity floor. The shape of the local Nusselt number profiles is similar to that predicted by Ooi *et al.* [17] with v^2-f and k-ε turbulence models. The Nusselt number is low just behind the upstream vertical cavity wall; it augments and then decreases again in vicinity of the downstream vertical wall. All profiles present a peak at each cavity corner within the secondary vortices regions. Two inflection points are observed at each secondary vortex region. A similar result has been observed by Hattori and Nagano [18], where the Stanton number profile presents two inflection points in the secondary vortex located behind 2-dimensional block. A similar result is also found by the numerical study of Ooi *et al.* [17] and that of Zdanski *et al.* [15]. This figure also shows that the augmentation of the Reynolds number and that of the turbulence intensity, enhance the heat transfer. The Reynolds number increase causes the flattening of the Nusselt number profiles. The maximum heat transfer occurs in the principal recirculation region, ahead of the reattachment region. This same phenomenon was observed by Zdanski *et al.* [15]. Likewise, the Numerical study of Hattori and Nagano [18] with the DNS method has shown that the maximum Stanton number points are located upstream of the reattachment points; results which agree, qualitatively, with the experimental data of Vogel and Eaton [19].

Figure 10 displays the maximum Nusselt number evolution along the cavity floor versus the turbulence intensity for different values of the Reynolds number. It is interesting to observe that the Nu_{max} increases linearly with the turbulence intensity. The maximum Nusselt number also increase with the Reynolds number.

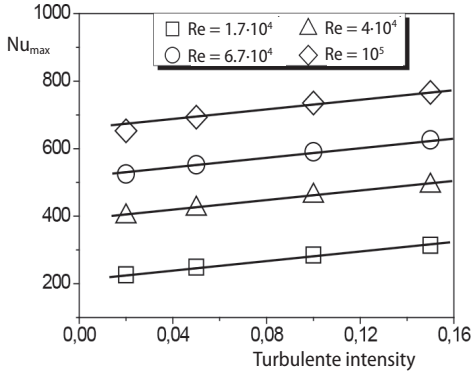

Figure 10. Evolution of the maximum Nusselt number as a function of Reynolds number and turbulence intensity

Effect of the cavity depth to nozzle height ratio in the wall jet incoming flow case

Computations of the wall jet upstream flow cases have been carried out for the same inlet flow conditions of the boundary layer case. Thus, at $x = -H$, $\delta \approx 20$ mm and $\mathrm{Re} = 67000$. The turbulence intensity is about 5%. The height of the outlet jet nozzle is maintained constant, equal to 50 mm whereas the cavity depth was varied while keeping an aspect ratio $AR = L/H$ equal to 10. Different cavity depths to nozzle height ratios are considered in this study: $H/b = 0.25$, 0.5, 0.67, 1, 1.5 and 2.

Figure 11 regroups the isotherms of the boundary layer incoming flow case and those of the wall jet incoming flow cases for five different cavity depth to nozzles height ratios. This figure shows that the higher temperatures are located in the vicinity of the upstream cavity corner, where the fluid remains trapped in the principal recirculation bubble. If comparing the isotherms of the boundary layer case and that of the wall jet for the same cavity depth ($H = b$), we note a significant decrease of the hot layer in the wall jet case. This is probably the consequence of the diminution of the principal recirculation bubble size. Madi Arous *et al.* [11] and Madi Arous *et al.* [16] showed an important decrease of the main recirculation bubble size and a shorter reattachment length when the incoming flow is that of a wall jet compared to that of the boundary layer. We also remark that the cavity depth increase induces a diminution of the hot fluid layer inside the cavity. However, this causes an amplification of the hot layer located over the downstream step. This figure reveals that the isotherms follow the streamlines behavior.

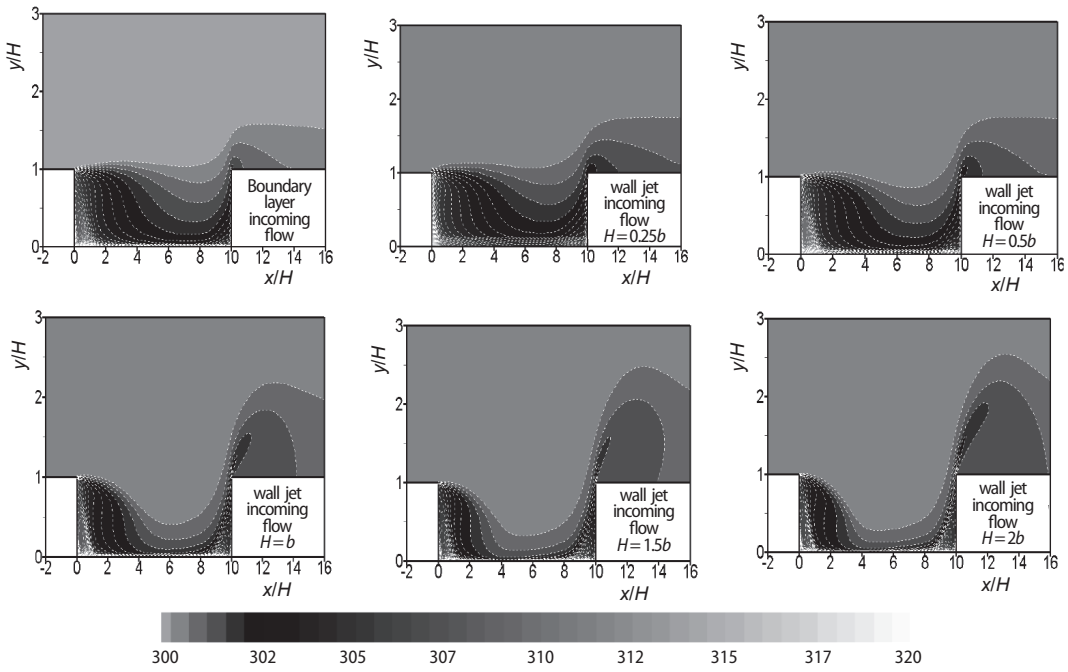

Figure 11. Isotherms for different cavity depth to nozzle height ratio (Re = 67000)

Figure 12 displays the temperature profiles at different cavities sections for three H/b ratios. The temperatures are highest near the cavity floor, and then decrease to reach the external flow temperature at about $y = H$. The temperatures are higher just behind the upstream step, then decrease inside the cavity. Increasing of the cavity depth to nozzles height ratio leads to a diminution of the temperatures values inside the cavity.

Figure 13 regroups the Nusselt number profiles along the cavity floor of the boundary layer incoming flow case and of the wall jet incoming flow case for the same cavity depth ($H = b = 50$ mm). Figure shows a considerable heat transfer enhancement in the wall jet case. Figure 14 regroups the Nusselt number profiles along the cavity floor of different cavity depth to nozzle height H/b ratios in the wall jet incoming flow case. We note that the augmentation of the cavity depth enhances the heat transfer between the heated cavity floor and the flow. This same

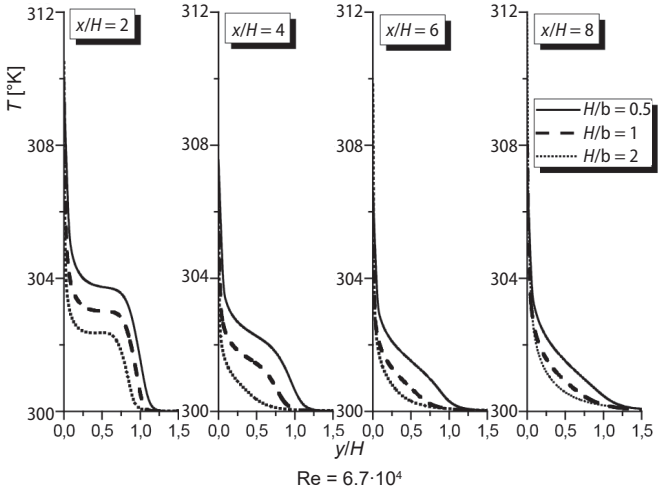

Figure 12. Temperature profiles at different sections for different cavity depth to nozzle height ratios (Re = 67000)

result was found by Abu-Mulaweh *et al.* [20] where their experimental study has shown that the step height increase enhances the heat transfer in the turbulent flow over a backward facing step. Apparently, the earlier reattachment phenomenon caused by the cavity depth augmentation Madi Arous *et al.* [11] and Madi Arous *et al.* [14] leads to an enhancement in a heat transfer between the heated cavity wall and the external fluid. A peak is observed in the vicinity of each vertical cavity wall; they are more important in the deepest cavity case.

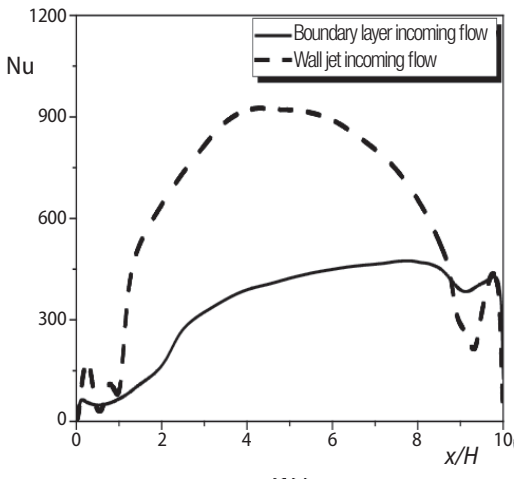

Figure 13. Nusselt number profile at the cavity floor (Comparison between boundary layer and wall jet incoming flows)

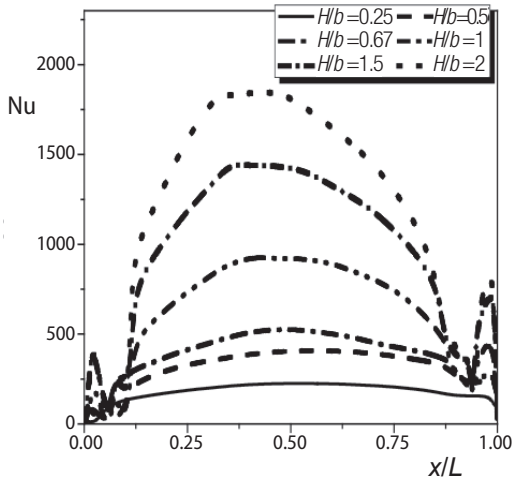

Figure 14. Nusselt number profiles at the cavity floor for different *H/b* ratios

Figure 15 illustrates the maximum Nusselt number evolution with the cavity depth. It is very interesting to note a linear increase of the maximum Nusselt number with the cavity depth.

Concluding remarks

A numerical approach of a turbulent flow over a shallow cavity is performed in this study. The numerical approach is based on the k-ω turbulence model. The comparison of the numerical results with the experimental ones shows that the k-ω model predicts fairly well this flow pattern. It was found that the flow structure is very sensitive to the upstream flow characteristics. The turbulence intensity increase accelerates the shear layer re-attachment to the cav-

ity floor and improves the heat transfer inside the cavity. The re-attachment phenomenon seems to be less affected by the Reynolds number. However, the increase of this latter enhances the heat transfer in the cavity. The wall jet incoming flow case is characterized by an earlier reattachment phenomenon and an enhancement in heat transfer as compared to that of the boundary layer. The augmentation of the cavity depth to nozzle height enhances even more the heat transfer. The maximum Nusselt number is reached upstream of the reattachment locations, in the principal recirculation region. This study reveals a linear evolution of the maximum Nusselt number with the turbulence intensity. The interesting result of this study is a linear evolution of the maximum Nusselt number with the cavity depth to the height of the jet exit nozzle.

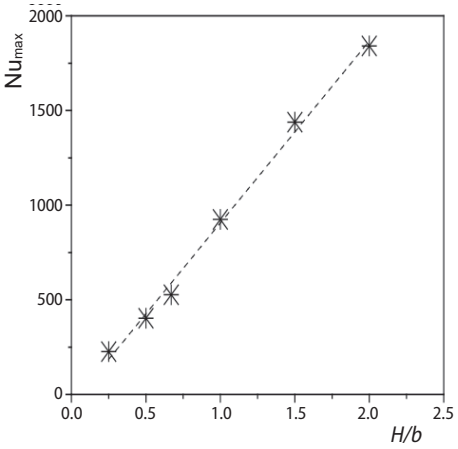

Figure 15. Evolution of the maximum Nu as a function of *H/b* ratio

Nomenclature

AR – cavity aspect ratio, (= L/H), [–]
b – nozzle height, [m]
C_f – skin friction coefficient, [–]
H – cavity depth, [m]
k – turbulence kinetic energy, [m²s⁻²]
L – cavity length, [m]
Nu – local Nusselt number, [–]
Nu_{max} – maximum Nusselt number, [–]
Re – Reynolds number, (= U_0H/ν), [–]
T_0 – external flow temperature, [K]
T_w – cavity walls temperature, [K]
U – streamwise velocity component, [ms⁻¹]
U_0 – maximum of U at $x = -H$, [ms⁻¹]
u – streamwise fluctuating velocity, [ms⁻¹]
V – vertical velocity component, [ms⁻¹]
v – vertical fluctuating velocity, [ms⁻¹]
x – streamwise co-ordinate, [m]
x_R – re-attachment length, [m]
y – vertical co-ordinate, [m]

Greek symbols

δ_{ij} – Kronecker delta, [–]
δ – boundary layer thickness, [m]
ν – kinematic viscosity, [m²s⁻¹]
ν_t – turbulent viscosity, [m²s⁻¹]
ρ – fluid density, [kgm⁻³]
ω – specific dissipation rate, [s⁻¹]

Reference

[1] Mehrez, Z., *et al.*, Mass Transfer Control of a Backward Facing Step Flow by Local Forcing Effect of Reynolds Number, *Thermal Science, 15* (2011), 2, pp. 367-378
[2] Lancial, N. *et al.*, Effect of a Turbolent Wall Jet on Heat Transfer over a Non-Confined Backward – Facing Step, *International Journal of Heat and Fluid Flow*, *44* (2013), Dec., pp. 336-347
[3] Mushatet Khudheyer, S., Simulation of Turbulent Flow and Heat Transfer with Ribs Turbulators, *Thermal Science, 15* (2011), 1, pp. 245-255
[4] Oka, S., Flow Field between Two Roughness Elements in Developed Turbulent Chanel Flow, in: *Heat and Mass Transfer in Flows with Separated Regions and Measurement Techniques*, Pergamon Press, New York, USA, 1972
[5] Richards, R. F., *et al.*,Turbulent Forced Convection Heat Transfer from a Bottom Heated Open Surface Cavity, *International Journal of Heat and Mass Transfer*, *30* (1987), 11, pp. 2281-2287
[6] Aung, W., An Interferometric Investigation of Separated Forced Convection in Laminar Flow Past Cavities, *Heat Transfer Journal*, *105* (1983), 1, pp. 505-512
[7] Bhatti, A., Aung W., Finite Difference Analysis of Laminar Separated Forced convection in cavities, *Journal of Heat Transfer*, *106* (1984), 1, pp. 49-54

[8] Delavar, M. A., *et al.*, Effect of Discret Heater at the Vertical Wall of the Cavity over Heat Transfer and Entropy Generation Using LBM, *Thermal Science*, *15* (2011), 2, pp. 423-435
[9] Stalio, E., *et al.*, Numerical Simultation of Forced Convection over a Periodic Series of Rectangular Cavities at Low Prandtl Number, *International journal of Heat and Fluid Flow*, *32* (2011), 5, pp. 1014-1023
[10] Esteve, M. J., *et al.*, Flow Field Characterisation within a Rectangular Cavity, *Proceedings*, 10th International Symposium on Applications of Laser Techniques to Fluid Mechanics, 2000, Lisbon, Portugal
[11] Madi Arous, F., *et al.*, Jet-Cavity Interaction: Effect of the Cavity Depth, *Progress in Computational Fluid Dynamics*, *11* (2012), 5, pp. 322-332
[12] Wilcox, D. C., *Turbulence Modelling for CFD,* DCW Industries, Inc., La Canada, Flintridge, Cal., USA, 1998
[13] Kader, B., Temperature and Concentration Profiles in Fully Turbulent Boundary Layers', *International Journal of Heat Mass Transfer*, *24* (1981), 9, pp. 1541-1544
[14] Avelar, A. C., *et al.*, Three-Dimensional Flow over Shallow Cavities, *Proceedings*,37th AIAA Fluid Dynamics Conference and Exhibit, Miami, Fla., USA, 2007
[15] Zdanski, P. S. B, *et al.*, Numerical Study of the Flow over Shallow Cavities, *Computers & Fluids*, *32* (2003), 7, pp. 953-974
[16] Madi Arous, F., *et al.*, Influence of Upstream Flow Characteristics on the Reattachment Phenomenon in Shallow Cavities, *Thermal Science*, *15* (2011), 3, pp. 721-734
[17] Ooi, A., *et al.*, Heat Transfer Predictions in Cavities, Center for Turbulence Research, Stanford University, Stanford, Cal., USA, 1998
[18] Hattori, H., Nagano, Y., Structure and Mechanism of Heat Transfer Phenomena in Turbulent Boundary Layer with Separation and Reattachment via DNS, *International Journal of Heat and Fluid Flow*, *37* (2012), Oct., pp. 81-92
[19] Vogel, J., Eaton, J., Combined Heat Transfer and Fluid Dynamics Measurements Downstream of a Backward Facing Step, *Journal of Heat Transfer*, *107* (1985), 4, pp. 922-929
[20] Abu-Mulaweh, H. I., *et al.*, Turbulent Mixed Convection Flow over a Backward Facing Step the Effect of the Step Heights, *International Journal of Heat and Fluid Flow*, *23* (2002), 6, pp. 758-765

Paper submitted: January 19, 2014
Paper revised: July 16, 2014
Paper accepted: July 17, 2014